High-Frequency Periodic Time-Domain Waveform Measurement System

MARKKU SIPILÄ, MEMBER, IEEE, KARI LEHTINEN, AND VEIKKO PORRA, MEMBER, IEEE

Abstract—A system is presented for the accurate measurement of high-frequency periodic time-domain voltage and current waveforms of a nonlinear microwave device. The measurements are performed in the time domain using a high-speed sampling oscilloscope. The results are Fourier transformed into the frequency domain for error correction and then back into the time domain. An error correction algorithm is presented enabling one to obtain accurate waveforms in spite of nonideal system components. Practical difficulties in measurement system characterization are also discussed. An accurate circuit model for the measurement fixture is developed and its element values are determined. Measurement results are given showing the waveforms in a microwave transistor operated in the nonlinear region. The errors caused by signal processing are discussed.

I. Introduction

In the study of nonlinear semiconductor devices, the best insight into the device behavior is often gained when the device operation is described in the time domain. At low frequencies the time-domain information is easily obtainable using conventional oscilloscopy. At UHF and microwave frequencies the situation is somewhat different. Active microwave devices in periodic nonlinear operation exhibit complex voltage and current waveforms with high harmonic content. If these waveforms could be measured accurately, valuable information would be obtained for the understanding and modeling of these devices. For example, if the nonsinusoidal voltages and currents in an MMIC power amplifier are measured, we gain considerable insight into the design of such amplifiers.

It is generally difficult to perform voltage and current waveform measurements at microwave frequencies. High-speed sampling oscilloscopes for periodic measurements have existed for a long time [1], but in the microwave region one has to take into account the errors caused by the frequency response of the measurement system, mismatches, multiple reflections, and other factors. Algorithms to correct these errors are widely used in connection with frequency-domain network analyzers [2]. They have also been used in large-signal measurements of nonlinear devices. Tucker and Bradley [3] describe a system for load-pull measurements with error correction. The system mainly deals with fundamental frequency information, in contrast with the system described in this report, which takes fully into account the influence of the harmonics.

Manuscript received October 29, 1987; revised May 4, 1988. This work was supported by Nokia-Mobira Oy, Salo, Finland, and by the Academy of Finland.

The authors are with the Electronic Circuit Design Laboratory, Faculty of Electrical Engineering, Helsinki University of Technology, Otakaari 5A, SF-02150 Espoo, Finland.

IEEE Log Number 8822912.

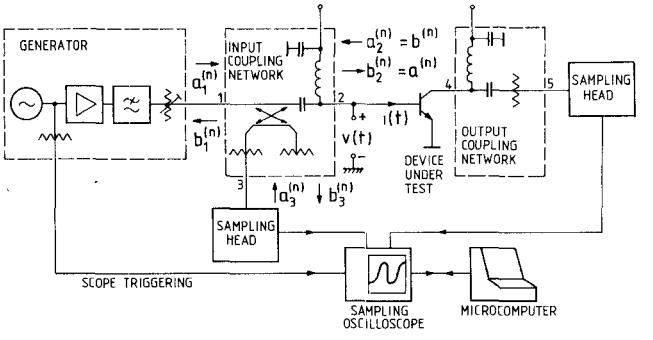

Fig. 1. Measurement system.

Time-domain network analyzers have been developed to measure the device S parameters using pulsed inputs [4], [5]. Scott and Smith describe such a system with error correction [6]. These analyzers require the device under test to be linear to give meaningful results.

It is required that the measurements be noninvasive, so that the measurement system does not disturb the quantities to be measured. A fast electro-optic sampling system was recently introduced to measure voltage waveforms noninvasively in GaAs chips [7]. In spite of its many advantages the system is limited to GaAs material. In addition, it requires expensive optical instrumentation and cannot be used to measure packaged devices.

In this paper we describe a time- and frequency-domain system for the accurate noninvasive measurement of periodic high-frequency voltage and current waveforms. The vector error correction algorithm employed allows one to take into account and correct the errors caused by losses, mismatches, and imperfect directivities in the measurement system. The system is equally suitable for measurements on packaged and unpackaged nonlinear devices of any material, and can be constructed using standard, commercially available equipment.

II. System Description

The measurement system for 2-port devices can be seen in Fig. 1. Let us suppose that we want to measure the periodic input and output voltage and current waveforms of a microwave transistor in the nonlinear region. The generator, consisting of a synthesized signal source, a

0018-9480/88/1000-1397$01.00 ©1988 IEEE

power divider, a linear power amplifier, a harmonic filter, and a step attenuator, feeds a sinusoidal input wave, which is incident on the device under test (DUT) and powerful enough to drive it into the nonlinear region. This gives rise to distorted voltage and current waveforms at the device ports. The distorted reflected wave is measured at port 3 of the input coupling network, using a fast sampling oscilloscope. The transmitted output waveform is simultaneously measured at port 5 of the output coupling network. When the S parameters of the linear input and output coupling networks are known at fundamental and harmonic frequencies, the accurate nonsinusoidal device waveforms can be determined by a microcomputer using the algorithm described below.

III. Waveform Determination

The periodic voltage and current at the device input port can be understood to consist of fundamental and harmonic waves $a^{(n)}$ and $b^{(n)}$ traveling into and out of the nonlinear DUT. The normalized wave variables are defined as follows:

$$a^{(n)} = \frac{V^{(n)} + Z_0 I^{(n)}}{2\sqrt{2Z_0}} \qquad b^{(n)} = \frac{V^{(n)} - Z_0 I^{(n)}}{2\sqrt{2Z_0}} \quad (1)$$

where Z_0 is the reference impedance (here 50 Ω for all harmonics), n is the order of the harmonic, and $V^{(n)}$ and $I^{(n)}$ are the nth Fourier coefficients of the DUT input voltage and current. It is our goal to determine these coefficients to obtain the DUT input waveforms. The wave variables are conventionally normalized so that the power carried by each wave is given by $|a^{(n)}|^2$ or $|b^{(n)}|^2$. The factor 2 under the square root is due to the fact that $V^{(n)}$ and $I^{(n)}$ are peak values, not rms values. For the definition of the wave variables, see [8].

The RF properties of the linear input coupling network can be described by its 3-port scattering matrix $\bar{\bar{S}}_i$:

$$(b_1 \quad b_2 \quad b_3)^T = \left(\bar{\bar{S}}_i\right)(a_1 \quad a_2 \quad a_3)^T \quad (2)$$

where the wave variables are defined in Fig. 1 and in (1). Equation (2) applies separately for each harmonic frequency $n\omega$, $n \geq 1$. The superscripts (n) are omitted for brevity in (2). At the moment we make the following simplifying assumptions, which can be partly relaxed later.

1) The generator and the sampling heads are perfectly matched for all $n\omega$ of importance, making $a_3^{(n)} = 0$ for all $n \geq 1$. If we cannot assume this, the mismatches can be accounted for by the procedure of Section IV.
2) The generator harmonic output is negligible. If this is not the case, the effect of the harmonics can be taken into account by a more elaborate analysis or it can be made negligible by using a low-pass-type input coupling network. Under these assumptions we can take $a_1^{(n)} = 0$, $n \geq 2$, for this analysis.
3) The gain of the sampling head is independent of frequency and its phase response is linear. This is a safe assumption if the highest harmonic frequency under consideration is well below the upper frequency limit of the sampling head. If this is not the case, the technique of Section IV can be used.
4) The sampling heads are operated in the linear region. This can be accomplished by using suitable attenuators in the coupling networks.
5) The dc bias ports of the input and output coupling networks are sufficiently isolated from the other ports, so that their terminations do not appreciably affect the S parameters of the network between the other ports. This can be accomplished by a proper design of the networks.
6) The load presented by the DUT at port 2 does not affect the generator output. A sufficient amount of attenuation or an isolator at the generator output must be used to ensure this.
7) The DUT is stable under large-signal excitation; i.e. it does not sustain oscillations at frequencies other than $n\omega$. The validity of this assumption can be checked by a spectrum analyzer at ports 3 and 5.

To obtain the DUT input waveforms, we first measure the periodic voltage $v_3(t)$ at port 3. Its complex Fourier coefficients $V_3^{(n)}$ are obtained from the digitized measurement results using the discrete Fourier transform:

$$V_3^{(n)} = \frac{1}{M}\sum_{m=0}^{M-1} v_3\left(\frac{mT}{M}\right)\exp\left(-\frac{j2\pi nm}{M}\right), \qquad n = 0,1,2,\cdots,N \quad (3)$$

where $T = 2\pi/\omega$ is the signal period. Voltage $v_3(t)$ is measured at intervals T/M, $M = 2N+1$, where N is the highest order of harmonics considered. The corresponding scattering variables are given by $b_3^{(n)} = V_3^{(n)}/\sqrt{2Z_0}$, applying (1) to port 3.

We also have to calibrate the system with the same generator output power by replacing the DUT with a known reflection coefficient and measuring the corresponding sinusoidal fundamental frequency wave $b_{3c}^{(1)} = b_{3c}$ at port 3.

To obtain the fundamental frequency waves $a^{(1)}(= b_2^{(1)})$ and $b^{(1)}(= a_2^{(1)})$ at the DUT input we proceed as follows.

The input coupling network, the DUT input, and the associated fundamental frequency wave variables are illustrated as a simplified signal flow diagram in Fig. 2. We define the nonlinear reflection coefficient ρ of the device under test as the ratio of the reflected and incident fundamental frequency waves at the DUT input:

$$\rho = \frac{b^{(1)}}{a^{(1)}} = \frac{b}{a} \quad (4)$$

following the notation of Fig. 1. From Fig. 2 we see that

$$b_3 = S_{31}a_1 + S_{32}b \quad (5)$$

and

$$a = S_{21}a_1 + S_{22}b. \quad (6)$$

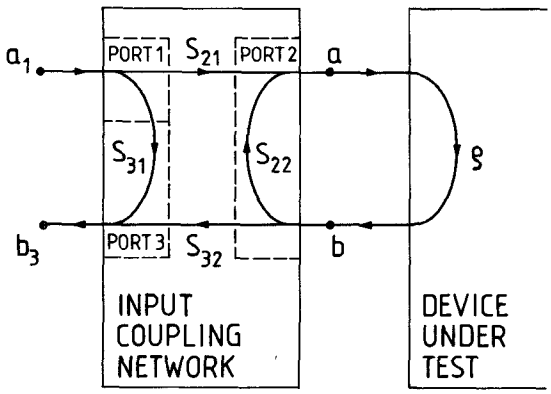

Fig. 2. Fundamental frequency wave variables in the input waveform measurement.

Here b_3 is known by measurement and subsequent Fourier analysis. Using (4), (5), and (6) we obtain

$$\rho = \frac{b_3 - S_{31}a_1}{S_{32}S_{21}a_1 + S_{22}(b_3 - S_{31}a_1)} \tag{7}$$

and b can now be determined from (5):

$$b = \frac{b_3 - S_{31}a_1}{S_{32}}. \tag{8}$$

Now it is easy to obtain a:

$$a = \frac{b}{\rho}. \tag{9}$$

All other quantities are assumed to be known, except a_1, the generator output wave. To express it in terms of port 3 quantities, an additional calibration measurement has to be made. We have to replace the DUT by a linear calibration standard with a known reflection coefficient ρ_c. After measuring the corresponding wave b_{3c} at port 3 we can solve (7) for a_1 as follows:

$$a_1 = \frac{b_{3c}(1 - S_{22}\rho_c)}{S_{31} + (S_{32}S_{21} - S_{22}S_{31})\rho_c}. \tag{10}$$

If a matched load ($\rho_c = 0$) is used as a calibration standard, (10) reduces to

$$a_1 = \frac{b_{3c}}{S_{31}}. \tag{11}$$

In the case of a short circuit ($\rho_c = -1$) we have

$$a_1 = \frac{b_{3c}(1 + S_{22})}{S_{31}(1 + S_{22}) - S_{32}S_{21}}. \tag{12}$$

Practical considerations determine which calibration standard is the best. Microstrip transmission lines are most often used to connect microwave devices into the measurement system, but it is not easy to realize high-quality microstrip calibration standards. In this case, however, only one standard is required.

We have now determined the fundamental frequency incident and reflected waves $a = a^{(1)}$ and $b = b^{(1)}$ at the DUT input ((7), (8), and (9)). To do this, we also needed the result of one calibration measurement to get a_1 from (10).

Next we have to determine the harmonic waves $a^{(n)}$ and $b^{(n)}$ ($n \geq 2$) at the DUT input. It was assumed that the generator harmonic output is negligible or the attenuation of the input coupling network at the harmonic frequencies is adequate to guarantee that the generator harmonics are not observable at ports 2 and 3. This is to ensure that all the harmonics measured at port 3 originate from the nonlinear device under test. When this assumption is valid, the harmonic wave $b^{(n)}$ can be obtained from the measured harmonic wave $b_3^{(n)}$ at port 3 simply by

$$b^{(n)} = \frac{b_3^{(n)}}{S_{32}^{(n)}} \tag{13}$$

and $a^{(n)}$ is given by

$$a^{(n)} = S_{22}^{(n)}b^{(n)} \tag{14}$$

where $S_{22}^{(n)}$ and $S_{32}^{(n)}$ are the scattering parameters of the input coupling network at the nth harmonic frequency.

If the assumption of negligible generator harmonics were not valid, one could perform, for each harmonic, a calibration procedure similar to that for the fundamental frequency above. The generator output waves $a_1^{(n)}$ would then be obtained; $a^{(n)}$ and $b^{(n)}$ at the DUT input could then be determined in exactly the same way as the fundamental waves above, using the S parameters at each harmonic frequency.

We have now determined both fundamental and harmonic waves at the DUT input. $V^{(n)}$ and $I^{(n)}$ can be obtained by solving (1):

$$V^{(n)} = \sqrt{2Z_0}\,(a^{(n)} + b^{(n)}) \tag{15}$$

$$I^{(n)} = \sqrt{\frac{2}{Z_0}}\,(a^{(n)} - b^{(n)}). \tag{16}$$

These equations apply for each harmonic separately. The total time-domain voltages $v(t)$ and currents $i(t)$ at time points mT/M are obtained by an inverse discrete Fourier transform:

$$v\left(\frac{mT}{M}\right) = \sum_{n=-N}^{N} V^{(n)} \exp\left(\frac{j2\pi nm}{M}\right), \quad m = 0,1,2,\cdots,M-1 \tag{17}$$

where

$$V^{(-n)} = (V^{(n)})^* \tag{18}$$

and

$$i\left(\frac{mT}{M}\right) = \sum_{n=-N}^{N} I^{(n)} \exp\left(\frac{j2\pi nm}{M}\right), \quad m = 0,1,2,\cdots,M-1 \tag{19}$$

where

$$I^{(-n)} = (I^{(n)})^*. \tag{20}$$

N is the highest order of harmonics considered, and must

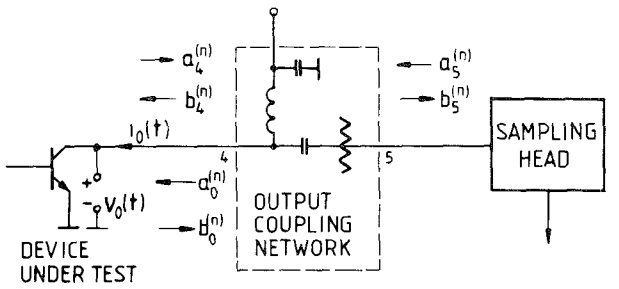

Fig. 3. Wave variables in the output waveform measurement.

be given a large enough value depending on the strength of the nonlinearity.

For 2-ports we also want to measure the device output waveform. The associated notation is given in Fig. 3. The two ports of the output coupling network are given the numbers 4 and 5 to distinguish them from the ports of the input coupling network. Here $a_o^{(n)}$ and $b_o^{(n)}$ are the wave variables to be determined at the device output. Assumptions 1, 3, 4, 5, 6, and 7 shall be valid in a way applicable to the output. It is not necessary to assume a sinusoidal generator output waveform when we are only interested in the DUT output waveform under prevailing conditions.

To determine the output voltage and current waveforms $v_o(t)$ and $i_o(t)$, the fundamental and harmonic waves $b_5^{(n)}$ are first obtained by sampling and Fourier analysis. It is then straightforward to determine the DUT output waves in a way analogous to (13) and (14):

$$b_o^{(n)} = \frac{b_5^{(n)}}{S_{54}^{(n)}} \tag{21}$$

$$a_o^{(n)} = S_{44}^{(n)} b_o^{(n)}. \tag{22}$$

This applies to both fundamental and harmonic waves. The waveforms $v_o(t)$ and $i_o(t)$ are then obtained by applying (15)–(20) to the output.

The method described can easily be applied to multiport networks by making the output waveform measurement at every output port in turn. The other ports have to be terminated with matched loads.

The dc components of the DUT terminal voltages and currents cannot be obtained in the same way as the ac components. They are, however, easily measurable at the bias ports of the input and output coupling networks. One must provide a low-resistance path between the DUT terminals and the bias ports and use adequate filtering to ensure that the RF voltages and currents do not affect the dc measurements. These goals are readily achievable by proper network design, in accordance with assumption 5.

IV. System Component Modeling

To obtain accurate measurement results we need to have reliable information about the characteristics of the measurement system. In particular, the S parameters of the coupling networks have to be known as accurately as possible.

It was assumed that the generator and the sampling heads are perfectly matched for all frequencies of importance. In reality this is not the case. We shall show how the mismatches can be taken into account so that the assumptions of this measurement method can be considered valid.

The situation at the input is illustrated in Fig. 4 using a signal flow diagram which applies to the fundamental and every harmonic frequency (superscripts (n) omitted for simplicity). The generator is described by its frequency-domain reflection coefficient $\rho_1 = \rho_1^{(n)} = \rho_1(n\omega)$, and the source wave $a_1' = a_1'^{(n)} = a_1(n\omega)$, defined as the wave obtained from the generator into a load Z_0 (here 50 Ω) so that $b_1 = 0$. According to assumption 2, $a_1'^{(n)} = 0$ for $n = 2, 3, \cdots$ but this is not absolutely necessary if a more elaborate analysis is performed according to Section III.

The sampling head is modeled using its small-signal reflection and transmission coefficients ρ_3 and τ_3 for each harmonic frequency $n\omega$, $n = 1, 2, 3, \cdots$. The coefficient τ_3 is defined as the voltage transfer coefficient between the input to the sampling head and the output display device.

Using the quantities of Fig. 4 we can define the S parameters of the reduced 3-port as follows:

$$S_{21}' = \frac{b_2}{a_1'}\bigg|_{a_2 = 0} \qquad S_{22}' = \frac{b_2}{a_2}\bigg|_{a_1' = 0}$$

$$S_{31}' = \frac{b_3'}{a_1'}\bigg|_{a_2 = 0} \qquad S_{32}' = \frac{b_3'}{a_2}\bigg|_{a_1' = 0}. \tag{23}$$

These quantities can be used in place of the corresponding unprimed S parameters in (5)–(14). They are given by

$$S_{21}' = \frac{S_{21} + (S_{23}S_{31} - S_{21}S_{33})\rho_3}{D} \tag{24}$$

$$S_{22}' = \frac{(1 - S_{33}\rho_3)(S_{22} - S_{11}S_{22}\rho_1 + S_{12}S_{21}\rho_1)}{D} - \frac{(S_{13}S_{22}S_{31} + S_{11}S_{23}S_{32} - S_{12}S_{23}S_{31} - S_{13}S_{21}S_{32})\rho_1\rho_3 - S_{23}S_{32}\rho_3}{D} \tag{25}$$

$$S_{31}' = \frac{S_{31}\tau_3}{D} \tag{26}$$

$$S_{32}' = \frac{S_{32}\tau_3 + (S_{12}S_{31} - S_{11}S_{32})\rho_1\tau_3}{D} \tag{27}$$

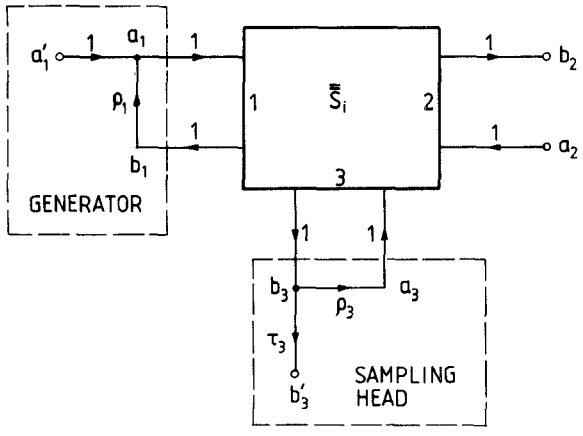

Fig. 4. Modeling of the nonidealities associated with the generator and the sampling head.

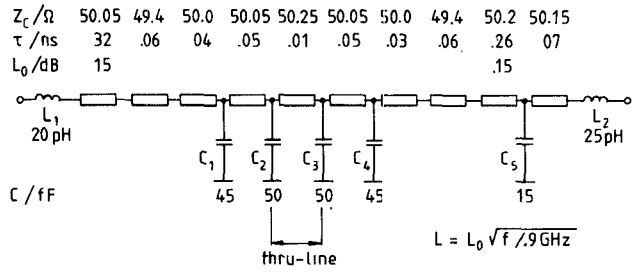

Fig. 5. Circuit model of transistor fixture HP 11608A with a through-line. Shown are the characteristic impedances Z_c, delays τ, and losses of the transmission line sections. The capacitances are given in femtofarads. L_0 is the total loss of a section in dB at 0.9 GHz ($L_0 = 0$ dB if not given). Frequency-dependent loss L used in the calculations is given by $L = L_0\sqrt{f/0.9\text{ GHz}}$, where f is the frequency in GHz.

where

$$D = (S_{11}S_{33} - S_{13}S_{31})\rho_1\rho_3 - S_{11}\rho_1 - S_{33}\rho_3 + 1. \quad (28)$$

These expressions can be derived by noting that $a_1 = a_1' + \rho_1 b_1$, $a_3 = \rho_3 b_3$, and $b_3' = \tau_3 b_3$. The insertion of these relations in the definition of the 3-port S parameters (2) results in a set of linear equations which can be solved for the reduced 3-port S parameter in question.

In the same way we can determine the reduced 2-port S parameters for the output coupling network. We obtain

$$S_{44}' = S_{44} + \frac{\rho_5 S_{45} S_{54}}{1 - \rho_5 S_{55}} \quad (29)$$

$$S_{54}' = \frac{S_{54}\tau_5}{1 - \rho_5 S_{55}} \quad (30)$$

where ρ_5 and τ_5 are the reflection and transmission coefficients, respectively, of the output sampling head.

Some difficulties may arise in the measurement of the generator and sampling head reflection and transmission coefficients. We briefly discuss these practical aspects here.

In order for $\rho_1^{(n)}$ to be well defined and measurable by a network analyzer, the generator output must be linear. If we cannot assume this, we run into difficulties. If the generator output is nonlinear, a load pull measurement could be made to determine the generator output power versus the load reflection coefficient. Unfortunately, the DUT input reflection coefficient ρ and the corresponding load seen by the generator are not known *a priori*, and we cannot determine the generator output power in the nonlinear case.

At the harmonic frequencies ($n = 2, 3, \cdots$) $\rho_1^{(n)}$ is made linear by the harmonic filter in the generator, so that $\rho_1^{(n)}$ is determined solely by the filter. The quantity $\rho_1^{(1)}$ can be linearized by inserting a sufficient amount of attenuation at the generator output.

The input reflection coefficient $\rho_3^{(n)}$ of the sampling head can be measured using a conventional network analyzer for the fundamental and harmonic frequencies as long as the signal level is low enough to ensure operation in the linear region. The quantity $\rho_3^{(n)}$ is time dependent because of the sampling process. For most of the time, however, the sampling diodes are not conducting, and we can use the associated measurable value for $\rho_3^{(n)}$.

It is more difficult to determine the transmission coefficient τ_3. Its absolute value can be found by applying an accurately calibrated input signal to the sampling head and by observing the corresponding output of the oscilloscope display. The phase of τ_3 is more difficult to determine. One possibility is to build an accurate electrical model for the sampling head [9]. A good approximation is to assume that $\tau_3^{(n)} = 1$ for frequencies well below the high end of the system operating band. The validity of this approximation can be tested at least for the magnitude of τ_3, as explained above.

The S parameters of most of the input and output coupling networks can be measured directly if the system components to be measured are equipped with suitable connectors, for example type APC-7. The coupling networks also include, however, a part of the transistor fixture, where the DUT is attached. We need to know the S parameters of the microwave networks between the fixture input and output connectors and the corresponding transistor reference planes. The DUT is usually connected to microstrip transmission lines, but because high-quality microstrip calibration standards are not readily available we cannot measure directly the S parameters of the network in question. Therefore we adopt the following method: The S parameters of the fixture with a through-line replacing the DUT are measured on a broad frequency band. The S parameters are transformed into the time domain using an inverse Fourier transform. The discontinuities along the fixture can now be identified using the information obtained from both input and output measurements [10]. When the discontinuities and the changes in characteristic impedance are known, the S parameters of the input and output networks can be calculated by frequency-domain circuit analysis. These calculated S parameters and the measured S parameters of other parts of the coupling networks can now be used to obtain the overall S parameters of the input and output coupling networks using conventional methods.

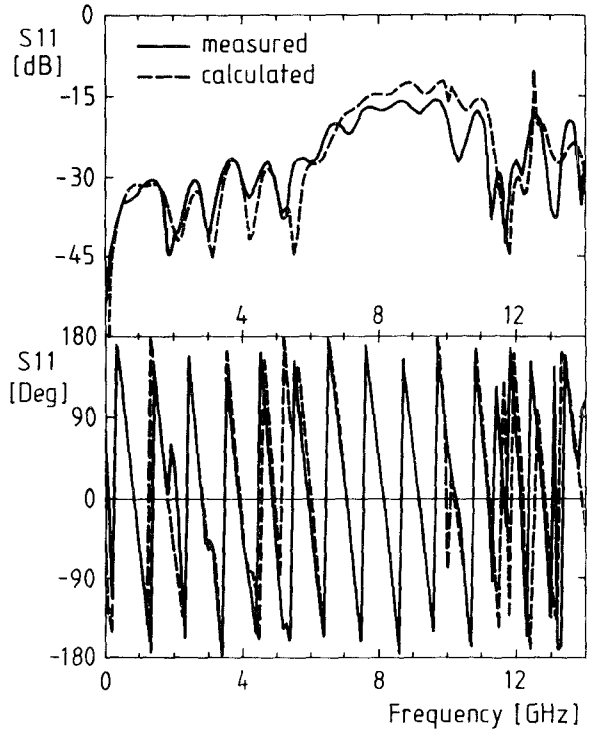

Fig. 6. Measured and calculated input reflection coefficient S_{11} magnitudes and phases of transistor fixture HP 11608A with a through-line. The discontinuity of phase at $\pm 180°$ is caused by the limited number of data points.

The circuit model obtained this way for the HP 11608A transistor fixture with a through-line is presented in Fig. 5. The measured and calculated magnitudes and phases of the fixture input reflection coefficient S_{11} are shown in Fig. 6. As can be seen, the measured and calculated results agree considerably well up to about 11 GHz, confirming that the circuit model is accurate. The agreement is also good in the transmission coefficient S_{21}, but in a well matched circuit such as this the consistency of the reflection coefficient is a better measure of the model accuracy, and therefore S_{11} is shown.

V. Measurements

The fundamental frequency $f = \omega/2\pi$ used in the measurements is limited by N, the highest order of harmonics considered, and the bandwidth of the sampling system. We use Tektronix S-4 sampling heads with a bandwidth of 14 GHz. Consequently $f \leqslant 2.8$ GHz if we choose $N = 5$.

The waveforms can also be measured inside a packaged microwave component or MMIC, on chip, if the package parasitics are known and they are not common to the input and the output. The input and output coupling networks are simply modified to include the parasitic elements by using a network analysis program. In the same way, for example, the matching circuits of a MMIC amplifier can be included, so that the waveforms inside the amplifier can be measured. The modified networks can be used in the calculations after $a_1^{(1)}$ has been determined using the unmodified input coupling network.

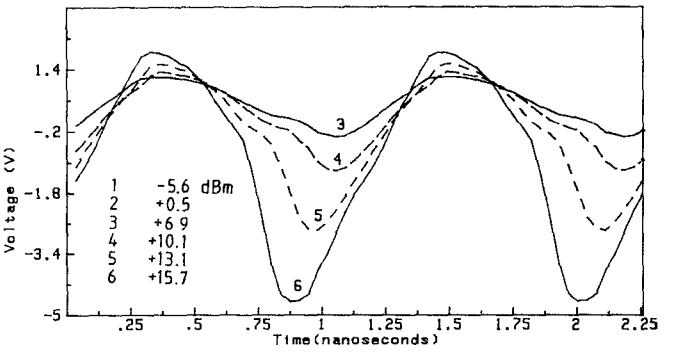

Fig. 7. Voltage waveform at input reference plane A_1 with the input power as parameter. The abbreviations of different input power levels are also given.

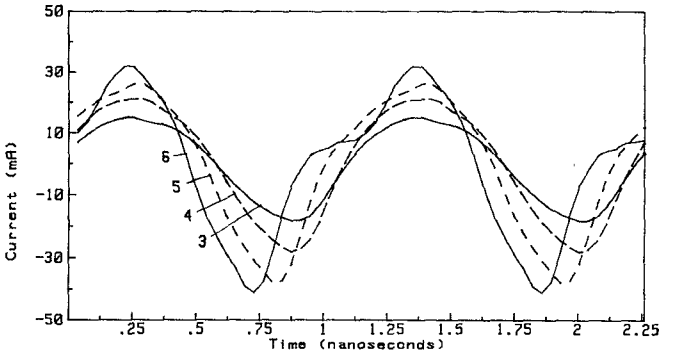

Fig. 8. Current waveforms at input reference plane A_1 with the input power as parameter (see Fig. 7).

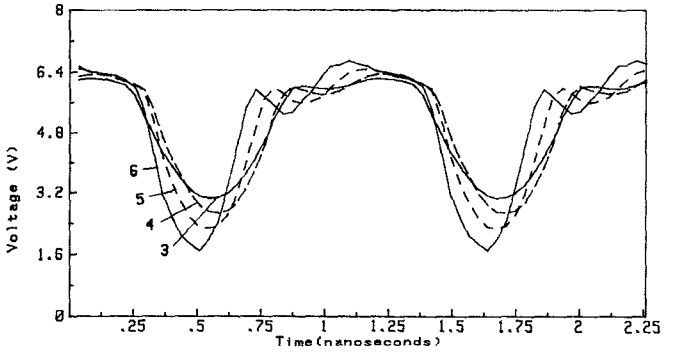

Fig. 9. Voltage waveforms at output reference plane A_2 with the input power as parameter (see Fig. 7).

The waveforms of wide-band bipolar transistor BFR93A ($f_T = 5$ GHz) were measured at several input power levels with $f = 0.9$ GHz. The time-domain voltages and currents are shown in Figs. 7–12. The given waveforms were measured at the inner (on chip) A_1–A_2 reference planes shown in Fig. 13. The associated parasitic and other elements are wire inductances L_{b1} and L_{b2}, the transmission lines with characteristic impedances Z_{c1} and Z_{c2} and delays τ_{d1} and

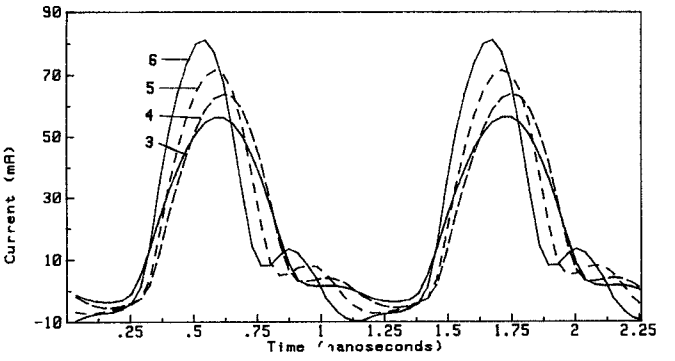

Fig. 10. Current waveforms at output reference plane A_2 with the input power as parameter (see Fig. 7).

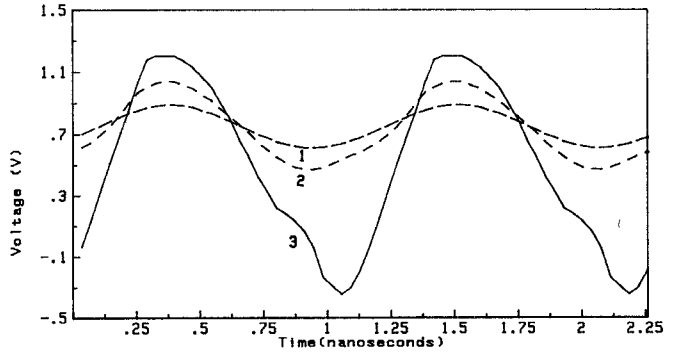

Fig. 11. Voltage waveforms at input reference plane A_1 with the input power as parameter (see Fig. 7), showing the transition into sinusoidal when the signal level is decreased. Note that the voltage waveforms at power level 3 in Figs. 7 and 11 are the same with different voltage scales.

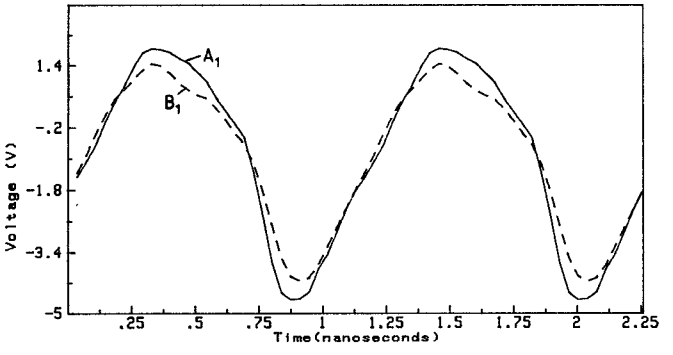

Fig. 12. Voltage waveforms at input reference planes B_1 and A_1, showing the effect of time-domain de-embedding at input power level 6 (+15.7 dBm).

τ_{d2} connecting the transistor to the fixture, and discontinuity inductances L_{d1} and L_{d2} and capacitances C_{d1} and C_{d2} due to the change in line width. The through-line of Fig. 5 was replaced by the network of Fig. 13 in real measurements. Note that C_{d1} and C_{d2} are not the same as C_2 and C_3 in Fig. 5, the latter being due to rubber clamps in the transistor fixture. The input power in dBm is used as a parameter in Figs. 7–11. It is defined as the fundamental

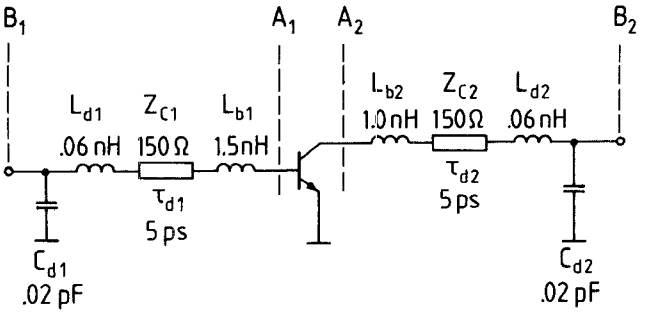

Fig. 13. Parasitic elements in the measurement of waveforms in transistor BFR93A, showing the inner (A_1-A_2) and outer (B_1-B_2) reference planes.

frequency power flowing towards the transistor in the input reference plane. The transistor was biased with collector current $I_c = 20$ mA and collector–emitter voltage $V_{CE} = 5$ V in small-signal conditions.

As can be seen in the measurement results, the transistor operation is highly nonlinear, especially at the higher power levels. Some interesting phenomena are revealed, for example the secondary peak in the output current at about 0.8 to 1.0 ns at the higher power levels in Fig. 10 or the strong asymmetry in the input current at power level 6 in Fig. 8. Such phenomena are not easily observable using conventional methods. In Fig. 11 the transition into linear operation at decreasing signal levels is shown. The voltage and current peaks and valleys are seen to be shifted as the power level is changed. This is a consequence of the change in the transistor parameters (for example in the effective input capacitance) as functions of power level. Fig. 12 gives the input voltage waveforms at two different input reference planes, A_1 and B_1. This is an example of the "time-domain de-embedding" made possible by this method.

VI. Sources of Error

After correcting the errors due to imperfect microwave hardware, some other sources of error remain. The remaining errors of the measurement system fall into three main categories, namely the errors caused by the oscilloscope scale nonlinearities, signal processing algorithms, and noise.

The oscilloscope introduces errors by the nonlinearity of its horizontal and vertical scales. They are usually small compared with other errors.

To discuss the errors caused by the signal processing, we briefly describe the practical aspects in the waveform acquisition. The displayed "raw" waveform measured was digitized at time intervals Δt = sweep time/512. The built-in PER feature of the Tektronix 7854 oscilloscope was used to find the signal period P as the time between two crossings in same direction across a certain voltage level. In general, P did not contain an integer number of time intervals Δt. The period used in the calculations was T, equal to the smallest integer multiple of Δt larger than P. With the settings of the preceding example $P/\Delta t \approx 114$, and the resulting worst case error in T was 0.88 percent. A small error in the signal period slightly distorts the wave-

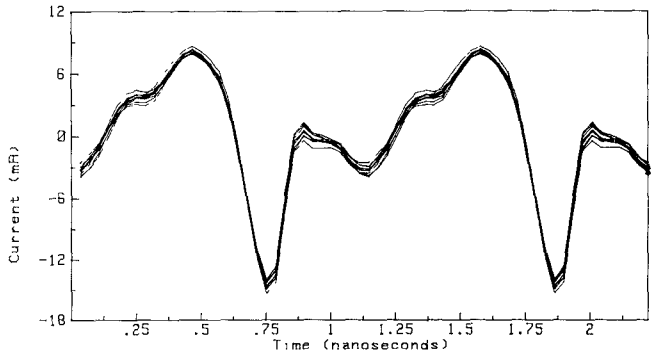

Fig. 14. Input current waveforms of Avantek AT-60585 bipolar transistor with the coupling network S parameters randomly varied. Bias point $I_c = 10$ mA and $V_{CE} = 8$ V in small-signal conditions, input power +11.9 dBm.

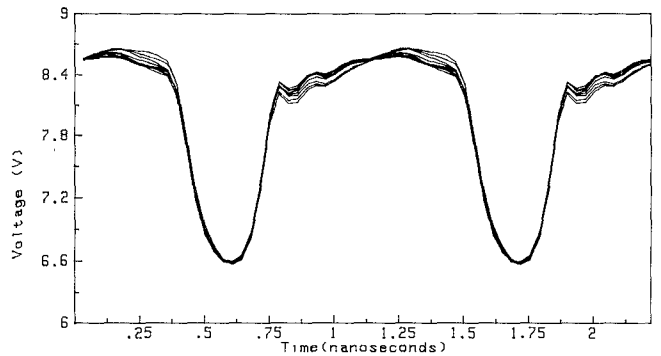

Fig. 15. Output voltage waveforms of Avantek AT-60585 bipolar transistor. Conditions are the same as in Fig. 14.

form measured. For example in the output this is manifested as a compression of the waveform by factor P/T (≈ 1) in the time scale. In critical applications this error can be minimized by choosing the oscilloscope time scale in such a way that the number of data points per period is maximized. Another possibility is to interpolate the data for discrete Fourier transform in order to create a new set of data points commensurable with the exact period P.

The aliasing error is caused by spectral components at frequencies higher than $N\omega$ affecting the Fourier coefficients at lower frequencies. N was chosen as large as the number of digitized voltage values permitted, in this case $N = 56$, corresponding to an upper frequency limit $N\omega/2\pi = 50.4$ GHz. Because of the finite bandwidth of the sampling system, the raw waveform did not contain frequencies appreciably higher than 14 GHz, resulting in negligible aliasing error.

The waveforms are also affected by noise. The effect of noise on the raw waveforms can be made very small by averaging the results of several (in this case 100) successive measurements, a feature of the Tektronix 7854 oscilloscope.

A more important noiselike contribution comes from the uncertainties in the coupling network S parameters and in the reflection coefficient ρ_c of the calibration standard. They affect the Fourier coefficients of the voltage and current, and potentially large errors can result after inverse discrete Fourier transform. To see how much the results are affected by these uncertainties, a Monte Carlo method was used to simulate the effect of S parameter errors on the waveforms. This kind of method would reveal the possible instabilities of the algorithm, i.e., large errors in the waveforms due to small errors in the Fourier coefficients. The coupling network S parameters were randomly varied in a Gaussian distribution with a standard deviation of 0.17 percent in the absolute value and 1.7° in the phase. These values represent typical measurement errors with an automatic network analyzer. Several (in this case ten) error correction calculations were performed with the same raw data. The resulting waveforms of AVANTEK AT-60585 bipolar transistor input current and output voltage are shown in Figs. 14 and 15. The maximum uncertainty is about ± 3.9 percent of the peak-to-peak input current and bout ± 4.2 percent of the peak-to-peak output voltage. No great loss of accuracy was observed.

VII. Conclusions

A method is presented which allows one to measure nonsinusoidal periodic voltage and current waveforms accurately at high frequencies. The measurements are made using a high-speed sampling oscilloscope giving the voltage waveform at a certain point of the measurement system. It is shown how the voltage and current waveforms at another point, for example at the input or output of a nonlinear device under test, can be obtained using Fourier transform and frequency-domain error correction techniques. The S parameters of the linear parts of the system must be known at the measurement frequency and its harmonics up to a sufficiently high order. These are partly measured and partly calculated from an accurate circuit model of the transistor fixture. It is also shown how the errors due to the generator and sampling head mismatches can be corrected.

The practical and conceptual difficulties encountered in the characterization of different parts of the measurement system are also discussed. A circuit model for the transistor fixture is developed. Measurement results are presented showing the voltage and current waveforms of microwave transistors in nonlinear operation. Finally, the errors which remain after the error correction procedure are discussed. They are mainly due to digital signal processing and inaccuracies in the coupling network S parameters.

These kinds of time-domain measurements are believed to be highly useful in providing insight into nonlinear design, in nonlinear modeling, and in validating existing nonlinear models of microwave devices. We have used the measurement system to study the accuracy of the Gummel Poon model in high-frequency bipolar transistor time-domain simulation.

Acknowledgment

The authors wish to express their thanks to Prof. M. Valtonen, T. Veijola, and K. Silvonen for many helpful discussions.

REFERENCES

[1] W. M. Grove, "Sampling for oscilloscopes and other RF systems: DC through *X*-band," *IEEE Trans. Microwave Theory Tech.*, vol. MTT-14, pp. 629–635, Dec. 1966.

[2] J. Fitzpatrick, "Error models for systems measurement," *Microwave J.*, pp. 63–66, May 1978.

[3] R. S. Tucker and P. D. Bradley, "Computer-aided error correction of large-signal load-pull measurements," *IEEE Trans. Microwave Theory Tech.*, vol. MTT-32, pp. 296–300, Mar. 1984.

[4] A. M. Nicolson, C. L. Bennett, D. Lamensdorf, and L. Susman, "Applications of time-domain metrology to the automation of broad-band microwave measurements," *IEEE Trans. Microwave Theory Tech.*, vol. MTT-20, pp. 3–9, Jan. 1972.

[5] J. R. Andrews, "Automatic network measurements in the time domain," *Proc. IEEE*, vol. 66, pp. 414–423, Apr. 1978.

[6] W. R. Scott, Jr., and G. S. Smith, "Error corrections for an automated time-domain network analyzer," *IEEE Trans. Instrum. Meas.*, vol. IM-35, pp. 300–303, Sept. 1986.

[7] B. H. Kolner and D. M. Bloom, "Electro-optic sampling in GaAs integrated circuits," *IEEE J. Quantum Electron.*, vol. QE-22, pp. 79–93, Jan. 1986.

[8] E. S. Kuh and R. A. Rohrer, *Theory of Linear Active Networks*. San Francisco: Holden-Day, 1967.

[9] S. M. Riad, "Modeling of the HP-1430A feedthrough wide-band (28-ps) sampling head," *IEEE Trans. Instrum. Meas.*, vol. IM-31, pp. 110–115, June 1982.

[10] T. Veijola and M. Valtonen, "Identification of cascaded microwave circuits with moderate reflections using reflection and transmission measurements," *IEEE Trans. Microwave Theory Tech.*, vol. 36, pp. 418–423, Feb. 1988.

Markku Sipilä (S'84–M'87) was born in Kerava, Finland, on November 5, 1955. He received the Diploma Engineer degree in 1981 and the Licentiate of Technology degree in 1987, both in electrical engineering, from the Helsinki University of Technology, Espoo, Finland.

From 1980 to 1984 he was with Mobira Oy, Salo, Finland, engaged in RF circuit and system design for cellular mobile radio. From 1984 to 1986 he was with Telecommunications Laboratory, Technical Research Centre of Finland (VTT), working on microwave techniques. Since 1986 he has been on leave from VTT with the Electronic Circuit Design Laboratory, Helsinki University of Technology, where he has been doing research on time-domain measurement techniques and on the modeling of nonlinear microwave devices. His research interests include various aspects of microwave circuits.

Kari Lehtinen was born in Turku, Finland, on April 9, 1962. He received the Diploma Engineer degree in electrical engineering in 1988 from the Helsinki University of Technology, Espoo, Finland. Since 1986 he has been with the Electronic Circuit Design Laboratory at the Helsinki University of Technology, where he is currently working on time-domain measurements at microwave frequencies.

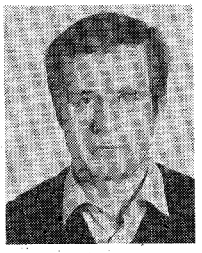

Veikko Porra (M'85) was born in Kannus, Finland, in 1938. He received the Diploma Engineer degree in 1961 and the Licentiate of Technology degree in 1966, both from the Helsinki University of Technology (HUT), Espoo, Finland.

From 1961 to 1967 he was a research engineer, from 1968 to 1985 an Associate Professor, and from 1972 to 1976 an Acting Professor in the Radio Laboratory of HUT. Since 1985 he has been a Professor of Electrical Engineering and the Head of the Electronic Circuit Design Laboratory at the university. During the academic year 1967–1968 he was a Visiting Scholar at the Polytechnic Institute of Brooklyn, Farmingdale. His research interests include parametric amplifiers, multiconductor transmission lines, and design methods for integrated circuits.